Supplementary Materials for

Redox stratification of an ancient lake in Gale crater, Mars

J. A. Hurowitz,* J. P. Grotzinger, W. W. Fischer, S. M. McLennan, R. E. Milliken, N. Stein, A. R. Vasavada, D. F. Blake, E. Dehouck, J. L. Eigenbrode, A.G. Fairén, J. Frydenvang, R. Gellert, J. A. Grant, S. Gupta, K. E. Herkenhoff, D. W. Ming, E. B. Rampe, M. E. Schmidt, K. L. Siebach, K. Stack-Morgan, D. Y. Sumner, R. C. Wiens

*Corresponding author. Email: joel.hurowitz@stonybrook.edu

Published 2 June 2017, *Science* **356**, eaah6849 (2017)
DOI: 10.1126/science.aah6849

This PDF file includes:

Other Supplementary Materials for this manuscript includes the following:
(available at www.sciencemag.org/content/356/6341/eaah6849/suppl/DC1)

Data File S1 (Excel)

Supplementary Text

The effect of S-bearing phases on CIA: On **Fig. S2**, we illustrate the effect on CIA of adding important S-bearing phases discussed in the text to mudstones of the Sheepbed member and the Murray formation, which include Mg-sulfate, Ca-sulfate, and airfall dust (approximated by APXS analyses of soil at Gale crater), which can coat rock surfaces to varying degrees. As shown, Mg-sulfate has no effect on CIA, but likely plays a role in causing diagenetic and high-SO_3 targets from the Murray HP facies (red squares) to scatter horizontally to the right on **Fig. S2** relative to the rest of the Murray HP facies (black circles). Ca-sulfate imparts a strong negative trajectory on **Fig. S2** to any sample that has been impacted by anyhydrite or gypsum addition (white squares). This effect is demonstrated by the APXS targets Mavor and Palmwag, which intentionally targeted Ca-sulfate veins in the Sheepbed member and Murray formation, respectively. In combination with Mg-sulfate, Ca-sulfate addition likely also plays a role in the offsetting the diagenetic and high-SO_3 HP facies targets from the rest of the Murray HP facies. The addition of dust coatings to the surfaces of rocks has the effect of drawing the samples towards total SO_3 values of ~5-10 wt. % and CIA of ~35%. The effects of dust coating are different for different mudstone compositions: for the Sheepbed member, dust contamination generates a horizontal vector on **Fig. S2**, because the CIA values of the Sheepbed mudstones are so similar to that of dust/soil. For the Murray formation (MS and HP facies), dust coatings will generate a vector with a negative slope, and therefore tend to mute the differences in CIA between the Murray formation and the Sheepbed member, while increasing total SO_3 concentration.

For both facies of the Murray formation some combination of Ca-sulfate addition (see also **Fig. 2**) and dust coating are implied, and the relationships displayed on **Fig. S2** indicate that the effects of these two processes would be difficult to disentangle from one another. Accordingly, rather than attempt an uncertain, and likely non-unique correction to CIA, we have chosen to compare "raw" CIA values. This represents a conservative approach to the treatment of CIA, as dust and/or Ca-sulfate removal calculations would only serve to amplify the differences in CIA between the mudstone suites. This is illustrated by a comparison of the difference between the average CIA of the Sheepbed member (34 ± 2%) and the Murray HP facies (45 ± 4%), which is 11%, and the difference between the CIA of the lowest SO_3 samples from the Sheepbed member (target Wernecke_brushed) and HP facies (target Topanga_DRT_Raster2), which is 16.1%.

Titanium and phosphorous distribution and mobility in the MS facies of the Murray fm.: One of the more enigmatic features that the MS facies exhibits is high concentrations of SiO_2 and TiO_2 and correlated behavior between the two oxides (**Fig. S3A**, **Table S1**), which might be interpreted to reflect a phase of post-depositional chemical weathering or diagenesis under low-pH conditions. On the basis of terrestrial analogue studies, weathering processes at low-pH are known to produce dramatic residual enrichment in SiO_2 and TiO_2 [e.g., (*87, 88*)]. These enrichments result from the insoluble nature of TiO_2 relative to the other cations leached from the host rock, and because silica can effectively behave as an immobile element under low pH conditions when silica concentrations are maintained at saturation with respect to amorphous silica. However, if

the MS facies underwent a phase of post-depositional alteration under low pH conditions, then one would also predict that CIA values should increase in concert with increasing SiO_2 and TiO_2; after all, CIA compares the behavior of a relatively insoluble element (Al) against a suite of highly soluble elements (Ca, Na, K), so CIA should behave in the expected manner unless stoichiometric mineral dissolution under highly corrosive conditions is invoked. Indeed, an examination of data from weathering rinds generated under low-pH conditions on a basalt sample from Hawaii [sample HWSB820, (*88*)] indicates that as TiO_2 and SiO_2 increase, CIA also increases dramatically, to values as high as 85% . This is in stark contrast to the behavior displayed by the MS facies, which exhibits low to moderate CIA values (**Fig. S3B**).

There are a number of potential mechanisms that could explain the observed geochemical enrichment of TiO_2 in the MS facies. One possibility is that TiO_2 was enriched as a result of redistribution during non-acidic diagenesis. Diagenetic TiO_2 mobilization and precipitation under marine pH conditions has been reported from a Cretaceous sedimentary basin on Earth (*89*). Perhaps related, experimental studies indicate that titanium mobility increases in the presence of phosphorous (*90, 91*), particularly at alkaline pH, and the MS facies is notable for elevated phosphorous concentration, ranging between 1.2 and 1.5 wt. % (**Data S1**). Fluorine also enhances the mobility of titanium in aqueous systems, as demonstrated by high temperature experimental studies (*92*), and fluorine has been observed as a conspicuous component of sedimentary rocks in Gale Crater using the ChemCam instrument, with both clastic and diagenetic carriers of fluorine implicated (*93*).

Another possibility is that the elevated TiO_2 observed in the MS facies is due to a provenance effect. There are no crystalline, high-TiO_2 content minerals that form an obvious repository to which elevated TiO_2 can be assigned in the MS facies (e.g., ilmenite, rutile, anatase), though if one of these phases were present just below the CheMin detection limit of ~1 wt. %, then they could account for some of the elevated TiO_2 (*43*). In addition, experimental studies indicate that synthetic cristobalite can incorporate 10 wt. % TiO_2 by solid solution (*94*), while synthetic tridymite has been observed to incorporate up to 1.25 wt. % TiO_2 as a substitutional impurity (*95*). Studies on terrestrial and extraterrestrial samples report that TiO_2 can approach 0.5-1.0 wt. % in natural tridymite and cristobalite (*96-98*). On this basis, we suggest that elevated TiO_2 in the MS facies may be explained by a combination of diagenetic titania redistribution in the presence of phosphate and fluorine, low abundance titanium-bearing detrital oxides, and substitutional incorporation of TiO_2 in the crystalline silica phases (tridymite, cristobalite) that are present in high abundance in this part of the Murray fm.

Lamination thickness measurements for Figure S5: The thickness and variability of lamination near targets investigated with the APXS instrument was characterized based on visual inspection of Mars Hand Lens Imager (MAHLI) and Mastcam images (*7, 99*), which are publically available on the Planetary Data System Catography and Imaging Sciences Node (img.pds.nasa.gov). APXS targets in the Murray Fm. with nearby well-expressed lamination were identified using Mastcam images. Although useful for identifying lamination, Mastcam images are often of insufficient resolution for accurate measurements of the mm-scale laminae in the Murray fm. because the stereoscopically derived scale of Mastcam images is on the order of cm. Instead, laminae were identified

visually in MAHLI images. Laminae thicknesses were calculated from the pixel separation between laminae centers along a transect drawn orthogonally through the mapped laminae. Thicknesses were measured orthogonally to bedding to account for the structural orientation of exposed blocks of Murray. The resolution of each image was approximated from the working distance of the MAHLI instrument, and computed thicknesses were corrected for instrument viewing angle when necessary. The arithmetic mean and one standard deviation in lamination thickness were computed for each target for comparison with FeO and SiO_2 weight percentages measured in-situ with the APXS instrument.

Another approach to examining the laminae is through wavelet analysis of grayscale pixel intensity in regions orthogonal to bedding. Due to the relatively small number (as low as 20-30) of countable laminae in some MAHLI images, the difficulty of distinguishing laminae from other mm-scale textures in some images via wavelet analysis, and artifacts resulting from image compression and stitching, only visual estimates of laminae were used to compute thicknesses. There are some additional caveats in the visual lamination thickness analysis. Thickness measurements were not corrected for surface variability such as undulations or recessed surfaces, which are typically negligible over the small field of view of MAHLI (5.0 x 3.7 cm at the nominal 5.0 cm standoff distance). Because lateral variations in lamination thickness were negligible, thicknesses were not averaged over multiple transects of the same laminae. In some images, sets of countable laminae are offset spatially by regions where laminae are not expressed. In these cases, different transects of each region contributed to the lamination thickness distribution for the same target.

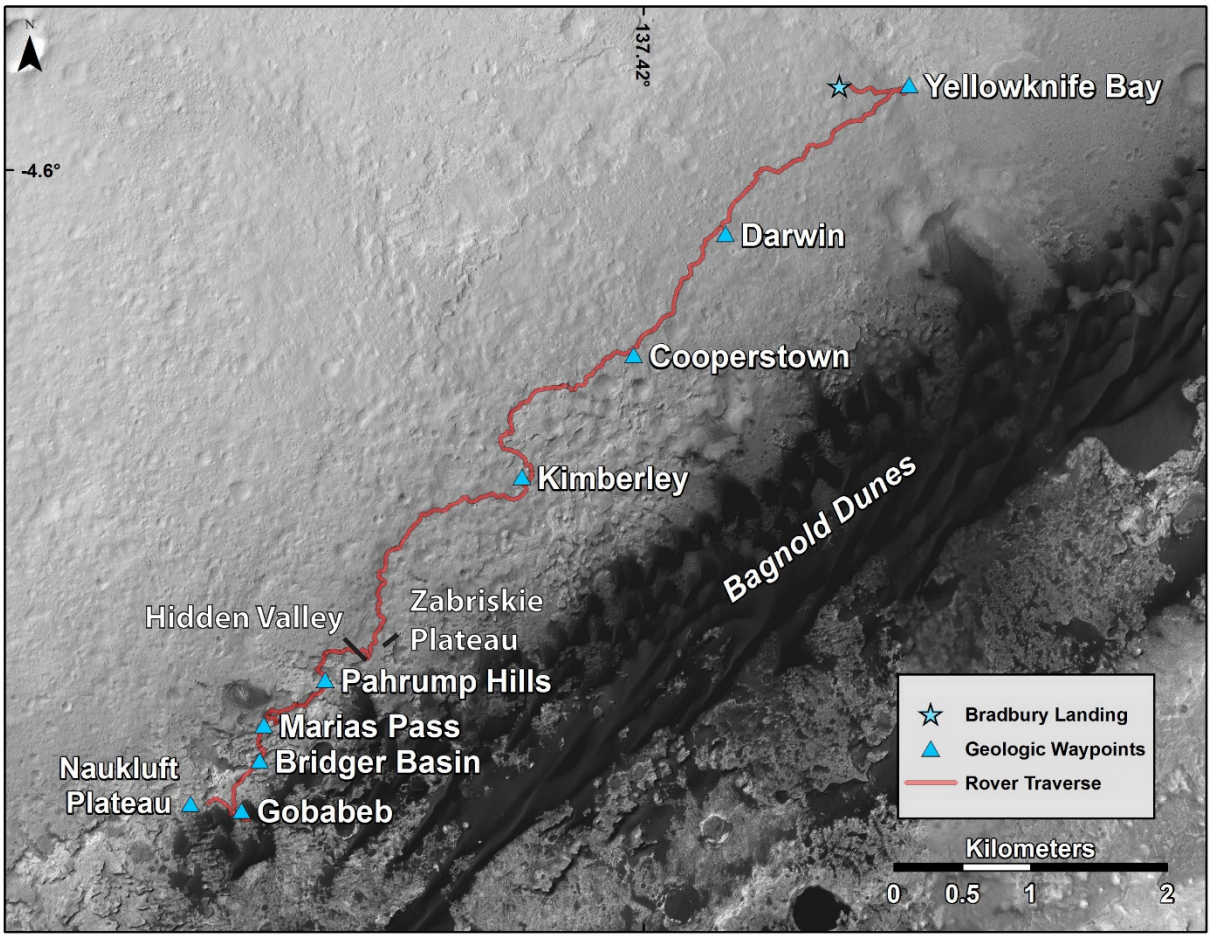

Figure S1: *Curiosity's* traverse across the floor of Gale crater. Major geological waypoints along the traverse between sols 1-1310 are identified. The Sheepbed member was investigated at the Yellowknife Bay waypoint. The investigation of the Murray fm. began at Hidden Valley, just southwest of the Zabriskie Plateau, and continued through Pahrump Hills, Marias Pass, Bridger Basin, Gobabeb, and up to the Naukluft Plateau, where the Stimson fm. unconformably overlies the Murray fm. Along the traverse, the Hematite-Phyllosilicate (HP) facies of the Murray fm. occurs primarily between Pahrump Hills and Marias Pass, and between Bridger Basin and the Naukluft Plateau. The Magnetite-Silica (MS) facies occurs at Hidden Valley, and between Marias Pass and Bridger Basin. The base image from the map is from the High Resolution Imaging Science Experiment Camera on NASA's Mars Reconnaissance Orbiter (Image Credit: NASA/JPL-Caltech/Univ. of Arizona).

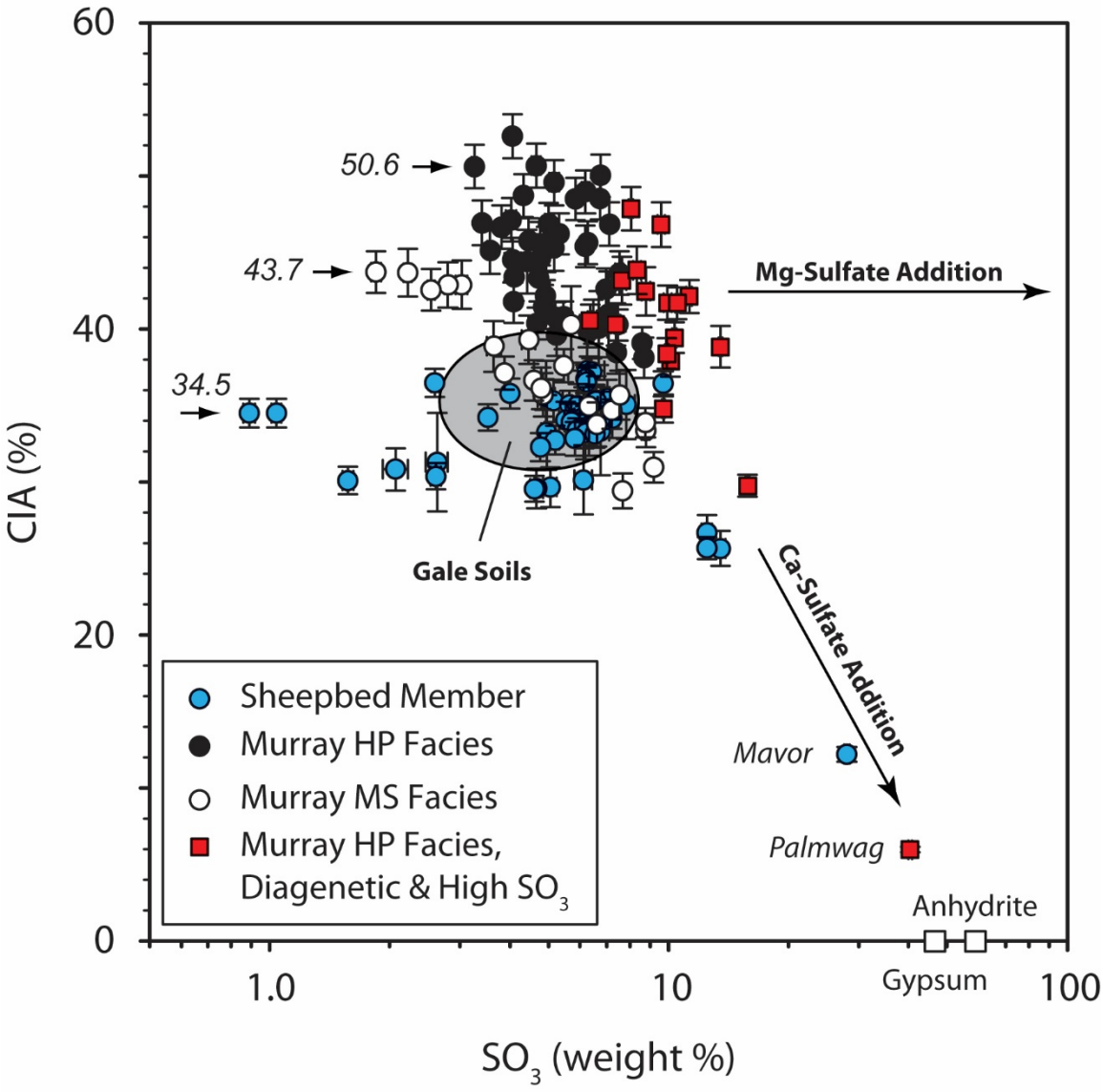

Figure S2: **The effects of S-bearing dust and minerals on CIA**. Vectors for the addition of Mg- and Ca-sulfate to mudstone samples shown on a plot of CIA (%) versus SO_3 (wt. %). The gray field represents the plotted positions of Gale Crater soils analyzed between sols 58-1184, used here as a proxy for the composition of airfall dust [see also (*39*)]. Arrowheaded lines with italicized CIA values reference the lowest SO_3 samples from the Sheepbed member, HP facies, and MS facies, which display a maximum difference of 16.1 %.

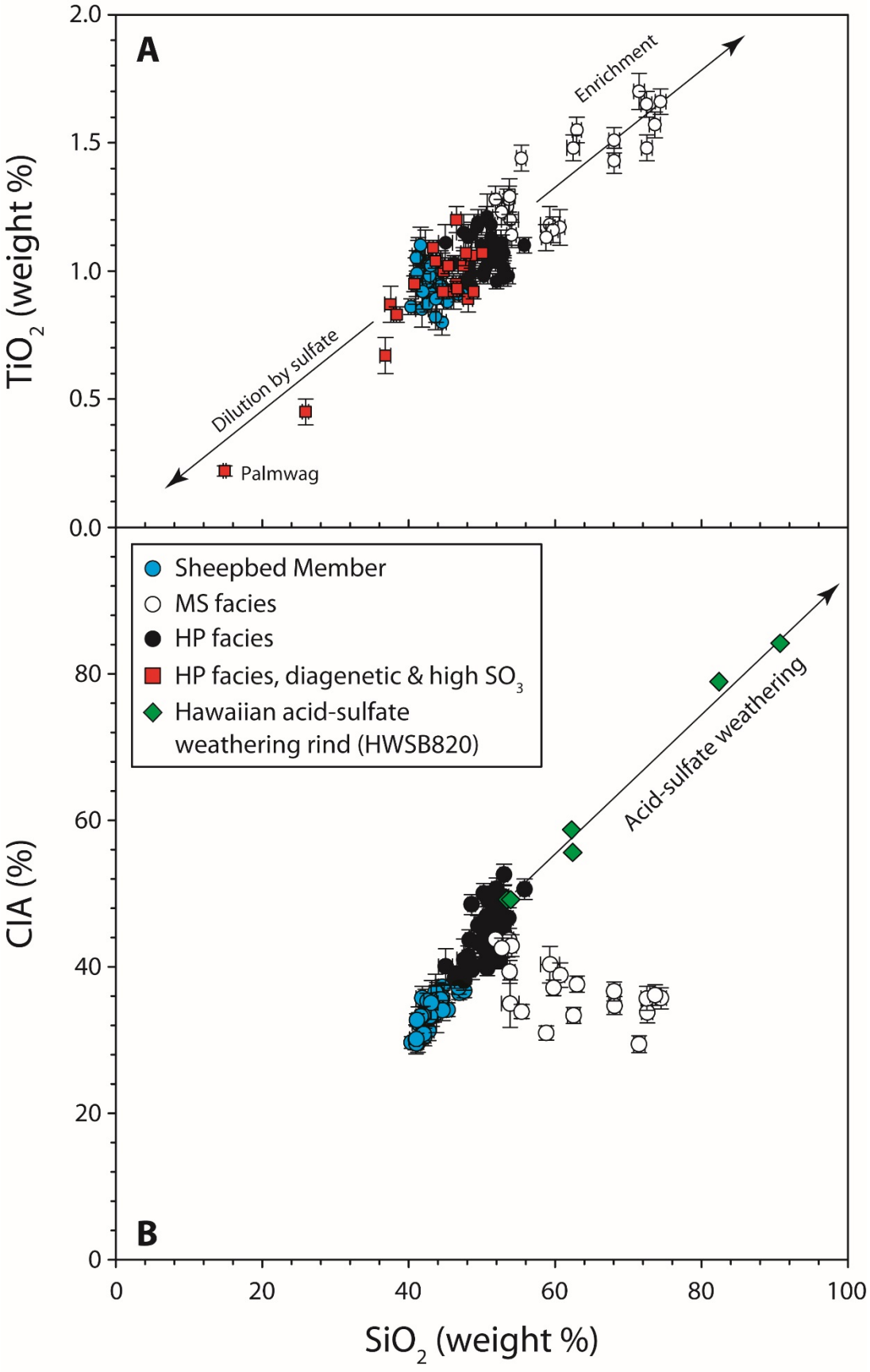
A
B
Enrichment
Dilution by sulfate
Palmwag
Acid-sulfate weathering
Sheepbed Member
MS facies
HP facies
HP facies, diagenetic & high SO3
Hawaiian acid-sulfate weathering rind (HWSB820)
TiO2 (weight %)
CIA (%)
SiO2 (weight %)
0.0
0.5
1.0
1.5
2.0
0
20
40
60
80
100

Figure S3 (previous page): **Redistribution of Si and Ti in the Murray formation.** (**A**) Plot of TiO_2 (wt. %) versus SiO_2 (wt. %) showing vectors for enrichment in these two elements in the MS facies, and dilution in diagenetic, high SO_3, and vein targets in the HP facies (see especially target Palmwag). Symbols as described for **Fig. 3** and **Fig. 4**. (**B**) Plot of CIA (%) versus SiO_2 (wt. %) demonstrating differences between the MS facies, affected by processes of silica and Ca-sulfate addition (also see **Fig. 2**), and acid-sulfate weathering of terrestrial basalts (*88*).

.

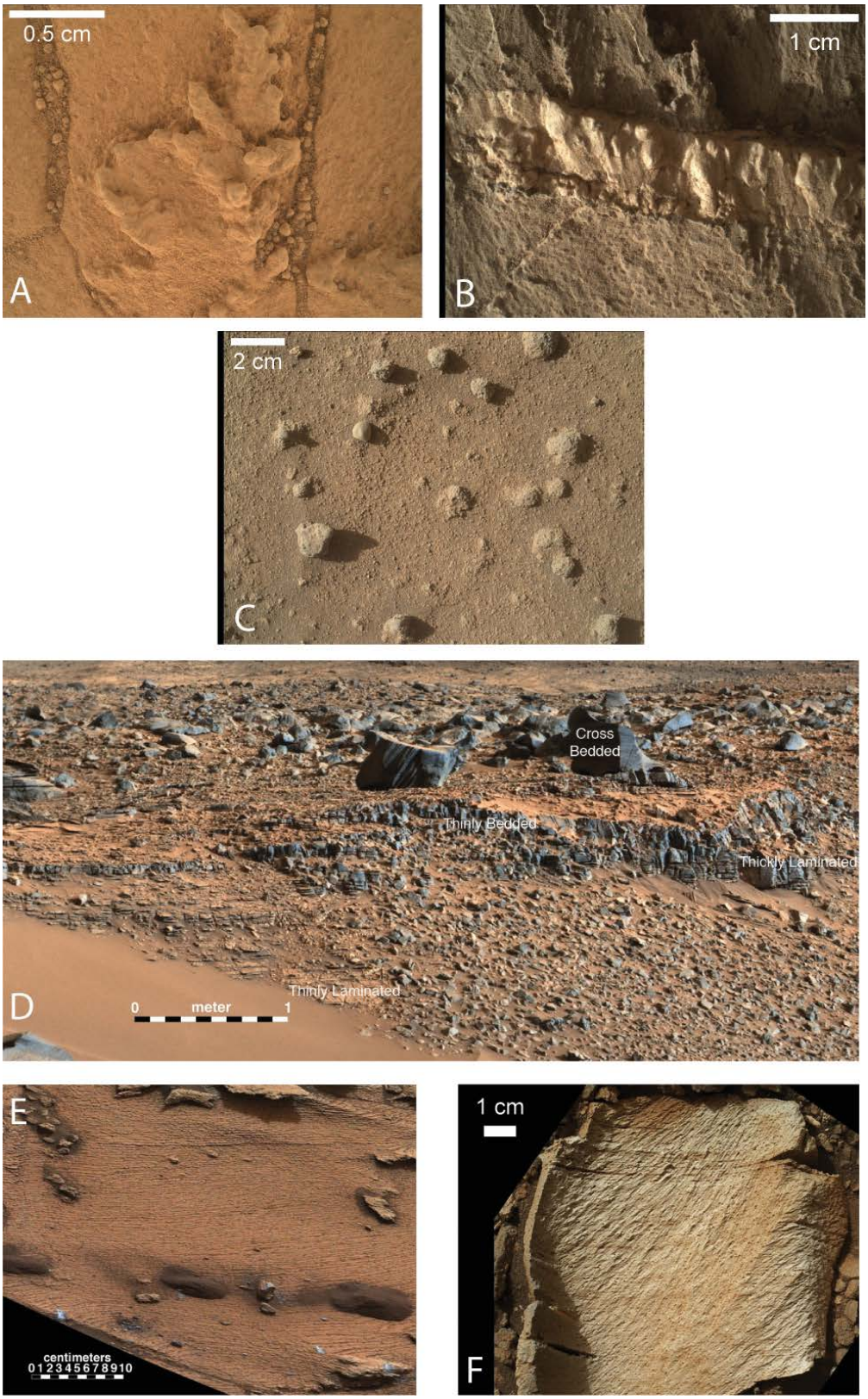
0.5 cm
A
1 cm
B
2 cm
C
Cross
Bedded
Thinly Bedded
Thickly Laminated
Thinly Laminated
D
0
meter
1
E
centimeters
0 1 2 3 4 5 6 7 8 9 10
1 cm
F

Figure S4 (previous page): **Sedimentological features of the Murray formation**. (**A**) MAHLI image of an MgO and SO_3-rich diagenetic feature at the base of the Murray fm. taken on sol 758 (image ID: 0758MH0001520010204633C00_DXXX. (**B**) MAHLI image of a Ca-sulfate vein (target Palmwag) cross-cutting the Murray fm., taken on sol 1,275 (image ID: 1275MH0005820010404440C00_DXXX). (**C**) MAHLI image of MgO and SO_3-rich diagenetic nodules in the Stimson fm., at the contact between the Murray and the Stimson, taken on sol 1,277 (image ID: 1277MH0001970010404560C00_DXXX). (**D**) Mastcam image taken of the walls of Hidden Valley on sol 703 showing cross-bedded fluvio-deltaic sandstones typical of the Zabriskie Plateau and Murray fm. mudstones displaying variable lamination and bedding thicknesses. Image reproduced from Fig. 6 of Grotzinger et al., (*10*), who interpret this image to represent a lacustrine facies overlain by laterally prograding fluvial-deltaic deposits. (**E**) Mastcam image of laminated Murray fm. mudstone from the HP facies, taken on sol 798 at Pahrump Hills. Image reproduced from Fig. 7B of Grotzinger et al. (*10*). Laminae are estimated to be ~2mm thick. (**F**) MAHLI image of the MS facies target "LaMoose", taken on sol 1041 (image ID: 1041MH0001900010400213C00). Laminae are estimated to be ~0.5mm thick. All images credited to: NASA/JPL-Caltech/MSSS.

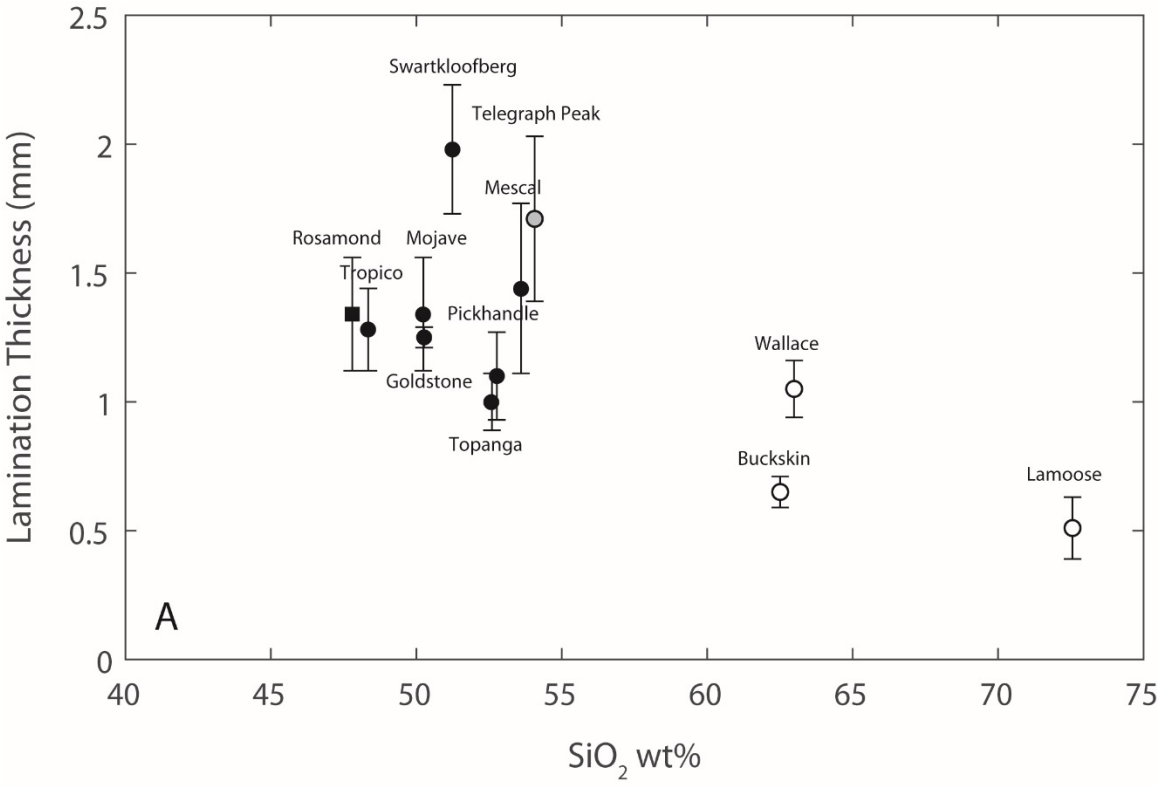
Lamination Thickness (mm)
SiO2 wt%
A
Swartkloofberg
Telegraph Peak
Mescal
Rosamond
Mojave
Tropico
Pickhandle
Goldstone
Topanga
Wallace
Buckskin
Lamoose

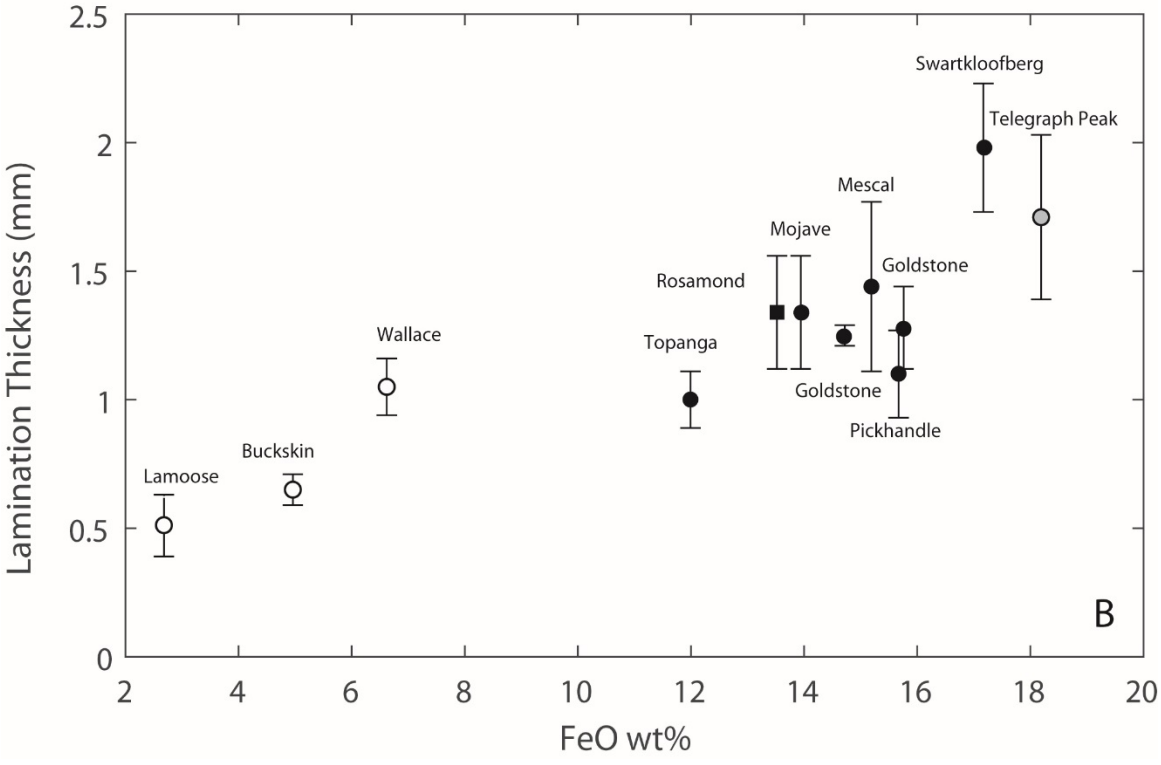
Lamination Thickness (mm)
FeO wt%
B
Swartkloofberg
Telegraph Peak
Mescal
Mojave
Goldstone
Rosamond
Topanga
Goldstone
Pickhandle
Wallace
Buckskin
Lamoose

Figure S5 (previous page): Relationships between bedding thickness and chemistry. (**A**) Plot of SiO_2 versus bedding thickness and (**B**) Total iron as FeO (FeO_T) versus bedding thickness, with target names identified. Symbols are the same as in **Figs. 3 and 4**. In (**B**), the sample Telegraph Peak is displaced to high FeO_T concentration relative to the other Murray MS samples plotted, possibly a consequence of the high concentration of magnetite (**Table S2**) of probable authigenic origin in this sample.

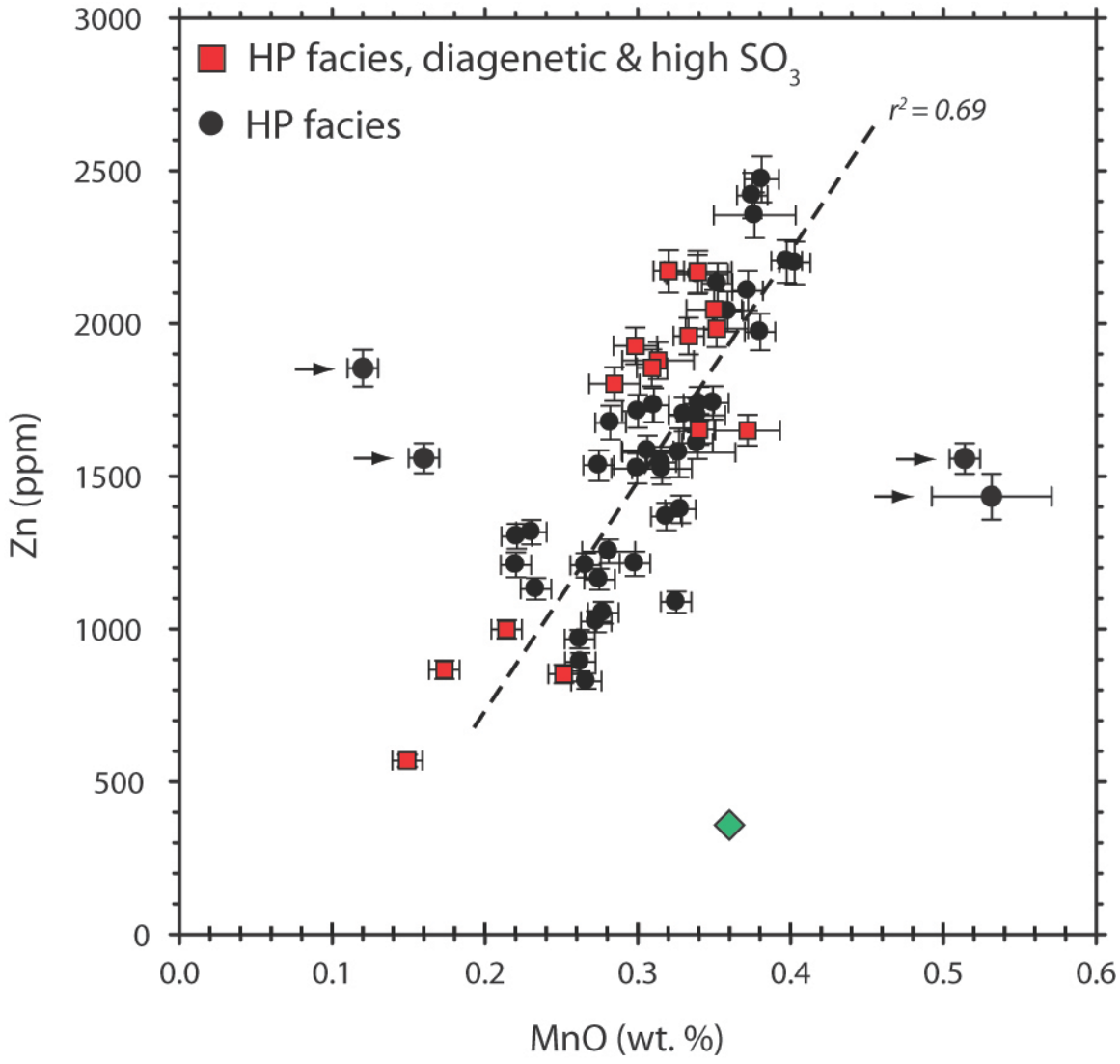

Figure S6: Mn-oxidation and Zn-concentration in diagenetic and high-SO_3 samples of the Murray HP facies. Zn (ppm) vs. MnO (wt. %) showing a linear regression for the HP facies that results from Mn-oxidation and scavenging of aqueous Zn by Mn-oxides (the outlier samples Ricardo_Raster_1, Ricardo_DRT_1, Kleinberg, and Schwarzrand, are excluded from the regression, labelled with arrowhead lines). Not included in the regression, but falling along the same trend, are diagenetic and high SO_3 samples from the HP facies. For these samples, either Mn-oxidation and Zn-scavenging continued during the later saline diagenesis, or MnO-Zn relationships in these targets were developed as a result of primary oxidative processes in the lake, but were not impacted by later saline diagenesis. Green diamond is average Martian crust.

Table S1. Mineralogical data from Gale Crater Mudstones

Mineral abundances with reported analytical uncertainties derived from CheMin XRD data. NR = not reported

	Sheepbed Member		Murray Fm			
Mineral (abun, %)	**John Klein**	**Cumberland**	**Confidence Hills**	**Mojave2**	**Telegraph Peak**	**Buckskin**
	Salts					
Anhydrite	2.3 (0.8)	0.9 (0.7)	0.0	0.0	0.0	0.7 (0.2)
Bassanite	1.2 (0.4)	1.3 (0.6)	0.0	0.0	0.0	0.0
Halite	0.4 (0.2)	0.1 (0.1)	0.0	0.0	0.0	0.0
Sum	*3.9*	*2.3*	*0.0*	*0.0*	*0.0*	*0.7*
	Amorphous					
Amorphous	30 (18)	30 (18)	39 (15)	53 (NR)	27 (15)	54 (NR)
	Clastic					
Plagioclase	23.7 (1.2)	22 (1.4)	20.4 (2.3)	23.5 (1.6)	27.1 (2.8)	17.1 (1.2)
Alkali feldspar	0.0	1.7 (0.9)	5.0 (0.7)	0.0	5.2 (2.2)	3.4 (0.7)
Augite	12.9 (1.1)	3.3 (1.2)	6.4 (2.2)	2.2 (1.1)	0.0	0.0
Orthopyroxene	0.0	5.7 (2.1)	2.1 (3.1)	0.0	3.4 (2.6)	0.0
Pigeonite	0.0	6.8 (1.8)	5.3 (1.7)	4.6 (0.7)	4.2 (0.1)	0.0
Forsterite	3.5 (0.7)	0.9 (0.8)	1.2 (0.7)	0.2 (0.8)	1.1 (1.2)	0.0
Ilmenite	0.4 (0.4)	0.3 (0.3)	0.0	0.0	0.0	0.0
Fluorapatite	0.0	0.0	1.3 (1.5)	1.8 (1.0)	1.9 (0.5)	0.0
Cristobalite	0.0	0.0	0.0	0.0	7.3 (1.7)	2.4 (0.3)
Quartz	0.4 (0.4)	0.0	0.7 (0.5)	0.8 (0.3)	0.9 (0.4)	0.0
Tridymite	0.0	0.0	0.0	0.0	0.0	13.6 (0.8)
Sum	*40.9*	*40.7*	*42.4*	*33.1*	*51.1*	*36.9*
	Secondary/Redox Sensitive					

Magnetite	3.3 (0.9)	4.4 (1.0)	3 (0.7)	3.0 (0.6)	8.2 (0.9)	2.8 (0.3)
Hematite	0.5 (0.5)	0.6 (0.5)	6.8 (1.5)	3.0 (0.6)	1.1 (0.5)	0.0
Akaganeite	1.1 (0.6)	1.8 (0.7)	0.0	0.0	0.0	0.0
Pyrite	0.4 (0.3)	0.0	0.0	0.0	0.0	0.0
Pyrrhotite	1 (0.5)	1.1 (0.6)	0.0	0.0	0.0	0.0
Jarosite	0.0	0.0	1.1 (0.7)	3.1 (1.6)	1.5 (1.8)	0.0
Opal-CT	0.0	0.0	0.0	0.0	10.9 (NR)	6.0 (NR)
Phyllosilicate	19 (9)	19 (9)	7.6 (NR)	4.7 (NR)	0.0	0.0
Sum	*25.3*	*26.9*	*19.3*	*13.8*	*21.7*	*8.8*

Plag: Pyx + Olivine	1.4	1.4	1.7	3.4	3.7	---

Data S1 (separate file). Geochemical Data from Gale Crater Mudstones and Soils.

Chemical abundances and CIA values with reported analytical uncertainties derived from APXS XRF data. Samples are subdivided into their appropriate formation, member, or facies and listed by target name with the sol number on which the data were collected.

References and Notes

1. H. W. Nesbitt, G. M. Young, Early Proterozoic climates and plate motions inferred from major element chemistry of lutites. *Nature* **299**, 715–717 (1982). doi:10.1038/299715a0

2. S. R. Taylor, S. M. McLennan, *The Continental Crust: Its Composition and Evolution*. A. Hallam, Ed. (Blackwell Scientific Publications, Oxford, 1985).

3. C. Klein, Some Precambrian banded iron-formations (BIFs) from around the world: Their age, geologic setting, mineralogy, metamorphism, geochemistry, and origin. *Am. Mineral.* **90**, 1473–1499 (2005). doi:10.2138/am.2005.1871

4. C. Fedo, H. W. Nesbitt, G. Young, Unraveling the effects of potassium metasomatism in sedimentary rocks and paleosols, with implications for paleoweathering conditions and provenance. *Geology* **23**, 921–924 (1995). doi:10.1130/0091-7613(1995)023<0921:UTEOPM>2.3.CO;2

5. W. W. Fischer, A. H. Knoll, An iron shuttle for deepwater silica in Late Archean and early Paleoproterozoic iron formation. *Geol. Soc. Am. Bull.* **121**, 222–235 (2009).

6. R. Anderson, J. I. Bell, Geologic mapping and characterization of Gale Crater and implications for its potential as a Mars Science Laboratory landing site. *Mars* **5**, 76–128 (2010).

7. J. P. Grotzinger, J. Crisp, A. R. Vasavada, R. C. Anderson, C. J. Baker, R. Barry, D. F. Blake, P. Conrad, K. S. Edgett, B. Ferdowski, R. Gellert, J. B. Gilbert, M. Golombek, J. Gómez-Elvira, D. M. Hassler, L. Jandura, M. Litvak, P. Mahaffy, J. Maki, M. Meyer, M. C. Malin, I. Mitrofanov, J. J. Simmonds, D. Vaniman, R. V. Welch, R. C. Wiens, Mars Science Laboratory Mission and science investigation. *Space Sci. Rev.* **170**, 5–56 (2012). doi:10.1007/s11214-012-9892-2

8. R. E. Milliken, J. P. Grotzinger, B. J. Thomson, Paleoclimate of Mars as captured by the stratigraphic record in Gale Crater. *Geophys. Res. Lett.* **37**, L04201 (2010). doi:10.1029/2009GL041870

9. B. J. Thomson, N. T. Bridges, R. Milliken, A. Baldridge, S. J. Hook, J. K. Crowley, G. M. Marion, C. R. de Souza Filho, A. J. Brown, C. M. Weitz, Constraints on the origin and evolution of the layered mound in Gale Crater, Mars using Mars Reconnaissance Orbiter data. *Icarus* **214**, 413–432 (2011). doi:10.1016/j.icarus.2011.05.002

10. J. P. Grotzinger, S. Gupta, M. C. Malin, D. M. Rubin, J. Schieber, K. Siebach, D. Y. Sumner, K. M. Stack, A. R. Vasavada, R. E. Arvidson, F. Calef 3rd, L. Edgar, W. F. Fischer, J. A. Grant, J. Griffes, L. C. Kah, M. P. Lamb, K. W. Lewis, N. Mangold, M. E. Minitti, M. Palucis, M. Rice, R. M. E. Williams, R. A. Yingst, D. Blake, D. Blaney, P. Conrad, J. Crisp, W. E. Dietrich, G. Dromart, K. S. Edgett, R. C. Ewing, R. Gellert, J. A. Hurowitz, G. Kocurek, P. Mahaffy, M. J. McBride, S. M. McLennan, M. Mischna, D. Ming, R. Milliken, H. Newsom, D. Oehler, T. J. Parker, D. Vaniman, R. C. Wiens, S. A. Wilson, Deposition, exhumation, and paleoclimate of an ancient lake deposit, Gale crater, Mars. *Science* **350**, aac7575 (2015). doi:10.1126/science.aac7575 Medline

11. J. P. Grotzinger, D. Y. Sumner, L. C. Kah, K. Stack, S. Gupta, L. Edgar, D. Rubin, K. Lewis, J. Schieber, N. Mangold, R. Milliken, P. G. Conrad, D. DesMarais, J. Farmer, K.

Siebach, F. Calef 3rd, J. Hurowitz, S. M. McLennan, D. Ming, D. Vaniman, J. Crisp, A. Vasavada, K. S. Edgett, M. Malin, D. Blake, R. Gellert, P. Mahaffy, R. C. Wiens, S. Maurice, J. A. Grant, S. Wilson, R. C. Anderson, L. Beegle, R. Arvidson, B. Hallet, R. S. Sletten, M. Rice, J. Bell 3rd, J. Griffes, B. Ehlmann, R. B. Anderson, T. F. Bristow, W. E. Dietrich, G. Dromart, J. Eigenbrode, A. Fraeman, C. Hardgrove, K. Herkenhoff, L. Jandura, G. Kocurek, S. Lee, L. A. Leshin, R. Leveille, D. Limonadi, J. Maki, S. McCloskey, M. Meyer, M. Minitti, H. Newsom, D. Oehler, A. Okon, M. Palucis, T. Parker, S. Rowland, M. Schmidt, S. Squyres, A. Steele, E. Stolper, R. Summons, A. Treiman, R. Williams, A. Yingst, MSL Science Team, A habitable fluvio-lacustrine environment at Yellowknife Bay, Gale crater, Mars. *Science* **343**, 1242777 (2014). doi:10.1126/science.1242777 Medline

12. L. Le Deit, E. Hauber, F. Fueten, M. Pondrelli, A. P. Rossi, R. Jaumann, Sequence of infilling events in Gale Crater, Mars: Results from morphology, stratigraphy, and mineralogy. *J. Geophys. Res.* **118**, 2439–2473 (2013). doi:10.1002/2012JE004322

13. M. C. Palucis, W. E. Dietrich, A. G. Hayes, R. M. E. Williams, S. Gupta, N. Mangold, H. Newsom, C. Hardgrove, F. Calef III, D. Y. Sumner, The origin and evolution of the Peace Vallis fan system that drains to the Curiosity landing area, Gale Crater, Mars. *J. Geophys. Res.* **119**, 705–728 (2014). doi:10.1002/2013JE004583

14. J. A. Grant, S. A. Wilson, N. Mangold, F. Calef III, J. P. Grotzinger, The timing of alluvial activity in Gale crater, Mars. *Geophys. Res. Lett.* **41**, 1142–1148 (2014). doi:10.1002/2013GL058909

15. T. Szabó, G. Domokos, J. P. Grotzinger, D. J. Jerolmack, Reconstructing the transport history of pebbles on Mars. *Nat. Commun.* **6**, 8366 (2015). doi:10.1038/ncomms9366 Medline

16. R. M. E. Williams, J. P. Grotzinger, W. E. Dietrich, S. Gupta, D. Y. Sumner, R. C. Wiens, N. Mangold, M. C. Malin, K. S. Edgett, S. Maurice, O. Forni, O. Gasnault, A. Ollila, H. E. Newsom, G. Dromart, M. C. Palucis, R. A. Yingst, R. B. Anderson, K. E. Herkenhoff, S. Le Mouélic, W. Goetz, M. B. Madsen, A. Koefoed, J. K. Jensen, J. C. Bridges, S. P. Schwenzer, K. W. Lewis, K. M. Stack, D. Rubin, L. C. Kah, J. F. Bell III, J. D. Farmer, R. Sullivan, T. Van Beek, D. L. Blaney, O. Pariser, R. G. Deen, MSL Science Team, Martian fluvial conglomerates at Gale crater. *Science* **340**, 1068–1072 (2013). doi:10.1126/science.1237317 Medline

17. M. Nachon, S. M. Clegg, N. Mangold, S. Schröder, L. C. Kah, G. Dromart, A. Ollila, J. R. Johnson, D. Z. Oehler, J. C. Bridges, S. Le Mouélic, O. Forni, R. C. Wiens, R. B. Anderson, D. L. Blaney, J. F. Bell III, B. Clark, A. Cousin, M. D. Dyar, B. Ehlmann, C. Fabre, O. Gasnault, J. Grotzinger, J. Lasue, E. Lewin, R. Léveillé, S. McLennan, S. Maurice, P.-Y. Meslin, W. Rapin, M. Rice, S. W. Squyres, K. Stack, D. Y. Sumner, D. Vaniman, D. Wellington, Calcium sulfate veins characterized by ChemCam/Curiosity at Gale crater, Mars. *J. Geophys. Res.* **119**, 1991–2016 (2014). doi:10.1002/2013JE004588

18. D. T. Vaniman, D. L. Bish, D. W. Ming, T. F. Bristow, R. V. Morris, D. F. Blake, S. J. Chipera, S. M. Morrison, A. H. Treiman, E. B. Rampe, M. Rice, C. N. Achilles, J. P. Grotzinger, S. M. McLennan, J. Williams, J. F. Bell III, H. E. Newsom, R. T. Downs, S. Maurice, P. Sarrazin, A. S. Yen, J. M. Morookian, J. D. Farmer, K. Stack, R. E. Milliken,

B. L. Ehlmann, D. Y. Sumner, G. Berger, J. A. Crisp, J. A. Hurowitz, R. Anderson, D. J. Des Marais, E. M. Stolper, K. S. Edgett, S. Gupta, N. Spanovich, MSL Science Team, Mineralogy of a mudstone at Yellowknife Bay, Gale crater, Mars. *Science* **343**, 1243480 (2014). doi:10.1126/science.1243480 Medline

19. R. J. Léveillé, J. Bridges, R. C. Wiens, N. Mangold, A. Cousin, N. Lanza, O. Forni, A. Ollila, J. Grotzinger, S. Clegg, K. Siebach, G. Berger, B. Clark, C. Fabre, R. Anderson, O. Gasnault, D. Blaney, L. Deflores, L. Leshin, S. Maurice, H. Newsom, Chemistry of fracture-filling raised ridges in Yellowknife Bay, Gale Crater: Window into past aqueous activity and habitability on Mars. *J. Geophys. Res.* **119**, 2398–2415 (2014). doi:10.1002/2014JE004620

20. K. L. Siebach, J. P. Grotzinger, L. C. Kah, K. M. Stack, M. Malin, R. Léveillé, D. Y. Sumner, Subaqueous shrinkage cracks in the Sheepbed mudstone: Implications for early fluid diagenesis, Gale crater, Mars. *J. Geophys. Res.* **119**, 1597–1613 (2014). doi:10.1002/2014JE004623

21. K. M. Stack, J. P. Grotzinger, L. C. Kah, M. E. Schmidt, N. Mangold, K. S. Edgett, D. Y. Sumner, K. L. Siebach, M. Nachon, R. Lee, D. L. Blaney, L. P. Deflores, L. A. Edgar, A. G. Fairén, L. A. Leshin, S. Maurice, D. Z. Oehler, M. S. Rice, R. C. Wiens, Diagenetic origin of nodules in the Sheepbed member, Yellowknife Bay formation, Gale crater, Mars. *J. Geophys. Res.* **119**, 1637–1664 (2014). doi:10.1002/2014JE004617

22. D. Blake, D. Vaniman, C. Achilles, R. Anderson, D. Bish, T. Bristow, C. Chen, S. Chipera, J. Crisp, D. Des Marais, R. T. Downs, J. Farmer, S. Feldman, M. Fonda, M. Gailhanou, H. Ma, D. W. Ming, R. V. Morris, P. Sarrazin, E. Stolper, A. Treiman, A. Yen, Characterization and calibration of the CheMin mineralogical instrument on Mars Science Laboratory. *Space Sci. Rev.* **170**, 341–399 (2012). doi:10.1007/s11214-012-9905-1

23. R. Gellert, R. Rieder, J. Brückner, B. C. Clark, G. Dreibus, G. Klingelhöfer, G. Lugmair, D. W. Ming, H. Wänke, A. Yen, J. Zipfel, S. W. Squyres, The Alpha Particle X-Ray Spectrometer (APXS): Results from Gusev Crater and calibration report. *J. Geophys. Res.* **111**, E02S05 (2006). doi:10.1029/2005JE002555

24. H. Bahlburg, N. Dobrzinski, in *Geological Record of Neoproterozoic Glaciations*, E. Arnaud, G. P. Halverson, G. Shields-Zhou, Eds. (Geological Society of London, 2011), vol. 36, pp. 81–92.

25. H. W. Nesbitt, in *Geochemistry of Sediments and Sedimentary Rocks: Evolutionary Considerations to Mineral Deposit-Forming Environments*, D. Lentz, Ed. (Geological Association of Canada, St. John's, 2002), vol. GEOText 4, pp. 39–51.

26. S. R. Taylor, S. M. McLennan, *Planetary Crusts: Their Composition, Origin and Evolution* (Cambridge Univ. Press, 2009).

27. S. M. McLennan, R. B. Anderson, J. F. Bell 3rd, J. C. Bridges, F. Calef 3rd, J. L. Campbell, B. C. Clark, S. Clegg, P. Conrad, A. Cousin, D. J. Des Marais, G. Dromart, M. D. Dyar, L. A. Edgar, B. L. Ehlmann, C. Fabre, O. Forni, O. Gasnault, R. Gellert, S. Gordon, J. A. Grant, J. P. Grotzinger, S. Gupta, K. E. Herkenhoff, J. A. Hurowitz, P. L. King, S. Le Mouélic, L. A. Leshin, R. Léveillé, K. W. Lewis, N. Mangold, S. Maurice, D. W. Ming, R. V. Morris, M. Nachon, H. E. Newsom, A. M. Ollila, G. M. Perrett, M. S. Rice, M. E.

Schmidt, S. P. Schwenzer, K. Stack, E. M. Stolper, D. Y. Sumner, A. H. Treiman, S. VanBommel, D. T. Vaniman, A. Vasavada, R. C. Wiens, R. A. Yingst, MSL Science Team, Elemental geochemistry of sedimentary rocks at Yellowknife Bay, Gale crater, Mars. *Science* **343**, 1244734 (2014). doi:10.1126/science.1244734 Medline

28. H. W. Nesbitt, G. M. Young, Prediction of some weathering trends of plutonic and volcanic rocks based on thermodynamic and kinetic considerations. *Geochim. Cosmochim. Acta* **48**, 1523–1534 (1984). doi:10.1016/0016-7037(84)90408-3

29. S. M. McLennan, Sedimentary silica on Mars. *Geology* **31**, 315–318 (2003). doi:10.1130/0091-7613(2003)031<0315:SSOM>2.0.CO;2

30. H. W. Nesbitt, R. E. Wilson, Recent chemical weathering of basalts. *Am. J. Sci.* **292**, 740–777 (1992). doi:10.2475/ajs.292.10.740

31. R. V. Morris, D. T. Vaniman, D. F. Blake, R. Gellert, S. J. Chipera, E. B. Rampe, D. W. Ming, S. M. Morrison, R. T. Downs, A. H. Treiman, A. S. Yen, J. P. Grotzinger, C. N. Achilles, T. F. Bristow, J. A. Crisp, D. J. Des Marais, J. D. Farmer, K. V. Fendrich, J. Frydenvang, T. G. Graff, J.-M. Morookian, E. M. Stolper, S. P. Schwenzer, Silicic volcanism on Mars evidenced by tridymite in high-SiO_2 sedimentary rock at Gale crater. *Proc. Natl. Acad. Sci. U.S.A.* **113**, 7071–7076 (2016). doi:10.1073/pnas.1607098113 Medline

32. N. Mangold, L. M. Thompson, O. Forni, A. J. Williams, C. Fabre, L. Le Deit, R. C. Wiens, R. Williams, R. B. Anderson, D. L. Blaney, F. Calef, A. Cousin, S. M. Clegg, G. Dromart, W. E. Dietrich, K. S. Edgett, M. R. Fisk, O. Gasnault, R. Gellert, J. P. Grotzinger, L. Kah, S. Le Mouélic, S. M. McLennan, S. Maurice, P.-Y. Meslin, H. E. Newsom, M. C. Palucis, W. Rapin, V. Sautter, K. L. Siebach, K. Stack, D. Sumner, A. Yingst, Composition of conglomerates analyzed by the Curiosity rover: Implications for Gale Crater crust and sediment sources. *J. Geophys. Res.* **121**, 353–387 (2016). doi:10.1002/2015JE004977

33. K. L. Siebach, M. B. Baker, J. P. Grotzinger, S. M. McLennan, R. Gellert, L. M. Thompson, J. A. Hurowitz, Sorting out compositional trends in sedimentary rocks of the Bradbury group (Aeolis Palus), Gale crater, Mars. *J. Geophys. Res.* **122**, 295–328 (2017). doi:10.1002/2016JE005195

34. A. H. Treiman, D. L. Bish, D. T. Vaniman, S. J. Chipera, D. F. Blake, D. W. Ming, R. V. Morris, T. F. Bristow, S. M. Morrison, M. B. Baker, E. B. Rampe, R. T. Downs, J. Filiberto, A. F. Glazner, R. Gellert, L. M. Thompson, M. E. Schmidt, L. Le Deit, R. C. Wiens, A. C. McAdam, C. N. Achilles, K. S. Edgett, J. D. Farmer, K. V. Fendrich, J. P. Grotzinger, S. Gupta, J. M. Morookian, M. E. Newcombe, M. S. Rice, J. G. Spray, E. M. Stolper, D. Y. Sumner, A. R. Vasavada, A. S. Yen, Mineralogy, provenance, and diagenesis of a potassic basaltic sandstone on Mars: CheMin X-ray diffraction of the Windjana sample (Kimberley area, Gale Crater). *J. Geophys. Res. Planets* **121**, 75–106 (2016). doi:10.1002/2015JE004932 Medline

35. V. Sautter, M. J. Toplis, R. C. Wiens, A. Cousin, C. Fabre, O. Gasnault, S. Maurice, O. Forni, J. Lasue, A. Ollila, J. C. Bridges, N. Mangold, S. Le Mouélic, M. Fisk, P.-Y. Meslin, P. Beck, P. Pinet, L. Le Deit, W. Rapin, E. M. Stolper, H. Newsom, D. Dyar, N.

Lanza, D. Vaniman, S. Clegg, J. J. Wray, *In situ* evidence for continental crust on early Mars. *Nat. Geosci.* **8**, 605–609 (2015). doi:10.1038/ngeo2474

36. R. W. Le Maitre, The chemical variability of some common igneous rocks. *J. Petrol.* **17**, 589–598 (1976). doi:10.1093/petrology/17.4.589

37. J. W. Tonkin, L. S. Balistrieri, J. W. Murray, Modeling sorption of divalent metal cations on hydrous manganese oxide using the diffuse double layer model. *Appl. Geochem.* **19**, 29–53 (2004). doi:10.1016/S0883-2927(03)00115-X

38. N. L. Lanza, R. C. Wiens, R. E. Arvidson, B. C. Clark, W. W. Fischer, R. Gellert, J. P. Grotzinger, J. A. Hurowitz, S. M. McLennan, R. V. Morris, M. S. Rice, J. F. Bell III, J. A. Berger, D. L. Blaney, N. T. Bridges, F. Calef III, J. L. Campbell, S. M. Clegg, A. Cousin, K. S. Edgett, C. Fabre, M. R. Fisk, O. Forni, J. Frydenvang, K. R. Hardy, C. Hardgrove, J. R. Johnson, J. Lasue, S. Le Mouélic, M. C. Malin, N. Mangold, J. Martìn-Torres, S. Maurice, M. J. McBride, D. W. Ming, H. E. Newsom, A. M. Ollila, V. Sautter, S. Schröder, L. M. Thompson, A. H. Treiman, S. VanBommel, D. T. Vaniman, M.-P. Zorzano, Oxidation of manganese in an ancient aquifer, Kimberley formation, Gale crater, Mars. *Geophys. Res. Lett.* **43**, 7398–7407 (2016). doi:10.1002/2016GL069109

39. J. A. Berger, M. E. Schmidt, R. Gellert, J. L. Campbell, P. L. King, R. L. Flemming, D. W. Ming, B. C. Clark, I. Pradler, S. J. V. VanBommel, M. E. Minitti, A. G. Fairén, N. I. Boyd, L. M. Thompson, G. M. Perrett, B. E. Elliott, E. Desouza, A global Mars dust composition refined by the Alpha-Particle X-ray Spectrometer in Gale Crater. *Geophys. Res. Lett.* **43**, 67–75 (2016). doi:10.1002/2015GL066675

40. S. J. VanBommel, R. Gellert, J. A. Berger, J. L. Campbell, L. M. Thompson, K. S. Edgett, M. J. McBride, M. E. Minitti, I. Pradler, N. I. Boyd, Deconvolution of distinct lithology chemistry through oversampling with the Mars Science Laboratory Alpha Particle X-Ray Spectrometer. *XRay Spectrom.* **45**, 155–161 (2016). doi:10.1002/xrs.2681

41. E. B. Rampe *et al*., Mineralogy of an ancient lacustrine mudstone succession from the Murray formation, Gale crater, Mars. *Earth Planet. Sci. Lett.* 10.1016/j.epsl.2017.04.021 (2017).

42. A. H. Treiman, R. V. Morris, D. G. Agresti, T. G. Graff, C. N. Achilles, E. B. Rampe, T. F. Bristow, D. W. Ming, D. F. Blake, D. T. Vaniman, D. L. Bish, S. J. Chipera, S. M. Morrison, R. T. Downs, Ferrian saponite from the Santa Monica Mountains (California, USA, Earth): Characterization as an analog for clay minerals on Mars with application to Yellowknife Bay in Gale Crater. *Am. Mineral.* **99**, 2234–2250 (2014). doi:10.2138/am-2014-4763

43. E. Dehouck, S. M. McLennan, P. Y. Meslin, A. Cousin, Constraints on abundance, composition, and nature of X-ray amorphous components of soils and rocks at Gale crater, Mars. *J. Geophys. Res.* **119**, 2640–2657 (2014). doi:10.1002/2014JE004716

44. H. Blatt, Provenance studies and mudrocks. *J. Sediment. Petrol.* **55**, 69–75 (1985).

45. D. B. Shaw, C. E. Weaver, The mineralogical composition of shales. *J. Sediment. Res.* **35**, 213–222 (1965).

46. J. Veizer, S. Jansen, Basement and sedimentary recycling and continental evolution. *J. Geol.* **87**, 341–370 (1979). doi:10.1086/628425

47. T. F. Bristow, D. L. Bish, D. T. Vaniman, R. V. Morris, D. F. Blake, J. P. Grotzinger, E. B. Rampe, J. A. Crisp, C. N. Achilles, D. W. Ming, B. L. Ehlmann, P. L. King, J. C. Bridges, J. L. Eigenbrode, D. Y. Sumner, S. J. Chipera, J. M. Moorokian, A. H. Treiman, S. M. Morrison, R. T. Downs, J. D. Farmer, D. D. Marais, P. Sarrazin, M. M. Floyd, M. A. Mischna, A. C. McAdam, The origin and implications of clay minerals from Yellowknife Bay, Gale crater, Mars. *Am. Mineral.* **100**, 824–836 (2015). doi:10.2138/am-2015-5077CCBYNCND

48. G. Schikorr, On the reactions between iron, its hydroxides and water. *Z. Elektrochem.* **35**, 65–70 (1929).

49. G. N. Schrauzer, T. D. Guth, Hydrogen evolving systems. 1. The formation of molecular hydrogen from aqueous suspensions of iron(II) hydroxide and reactions with reducible substrates, including molecular nitrogen. *J. Am. Chem. Soc.* **98**, 3508–3513 (1976). doi:10.1021/ja00428a019

50. A. Stefánsson, S. Amórsson, A. E. Sveinbjörnsdóttir, Redox reactions and potentials in natural waters at disequilibrium. *Chem. Geol.* **221**, 289–311 (2005). doi:10.1016/j.chemgeo.2005.06.003

51. B. L. Ehlmann, J. Buz, Mineralogy and fluvial history of the watersheds of Gale, Knobel, and Sharp craters: A regional context for the Mars Science Laboratory Curiosity's exploration. *Geophys. Res. Lett.* **42**, 264–273 (2015). doi:10.1002/2014GL062553

52. C. N. Alpers, J. L. Jambor, D. K. Nordstrom, Eds., *Sulfate Minerals: Crystallography, Geochemistry, and Environmental Significance* (Mineralogical Society of America and The Geochemical Society, Washington, DC, 2000), vol. 40, p. 606.

53. R. G. Burns, D. S. Fisher, Rates of oxidative weathering on the surface of Mars. *J. Geophys. Res.* **98**, 3365–3372 (1993). doi:10.1029/92JE02055

54. L. J. McHenry, V. Chevrier, C. Schroder, Jarosite in a Pleistocene East African saline-alkaline paleolacustrine deposit: Implications for Mars aqueous geochemistry. *J. Geophys. Res.* **116**, E04002 (2011). doi:10.1029/2010JE003680

55. D. T. Vaniman, S. J. Chipera, D. L. Bish, Pedogenesis of siliceous calcretes at Yucca Mountain, Nevada. *Geoderma* **63**, 1–17 (1994). doi:10.1016/0016-7061(94)90106-6

56. P. M. Dove, in *Chemical Weathering Rates of Silicate Minerals*, A. F. White, S. L. Brantley, Eds. (Mineralogical Society of America, Chantilly, VA, 1995), vol. 31, pp. 235–290.

57. W. Stumm, B. Sulzberger, The cycling iron in natural environments: Considerations based on laboratory studies of heterogeneous redox processes. *Geochim. Cosmochim. Acta* **56**, 3233–3257 (1992). doi:10.1016/0016-7037(92)90301-X

58. P. F. Hoffman, A. J. Kaufman, G. P. Halverson, D. P. Schrag, A neoproterozoic snowball earth. *Science* **281**, 1342–1346 (1998). doi:10.1126/science.281.5381.1342 Medline

59. G. P. Halverson, F. Poitrasson, P. F. Hoffman, A. Nédélec, J.-M. Montel, J. Kirby, Fe isotope and trace element geochemistry of the Neoproterozoic syn-glacial Rapitan iron formation. *Earth Planet. Sci. Lett.* **309**, 100–112 (2011). doi:10.1016/j.epsl.2011.06.021

60. N. J. Beukes, C. Klein, in *The Proterozoic Biosphere: A Multidisciplinary Study*, J. W. Schopf, C. Klein, Eds. (Cambridge Univ. Press, 1990), pp. 147–151.

61. G. M. Cox, G. P. Halverson, W. G. Minarik, D. P. Le Heron, F. A. Macdonald, E. J. Bellefroid, J. V. Strauss, Neoproterozoic iron formation: An evaluation of its temporal, environmental and tectonic significance. *Chem. Geol.* **362**, 232–249 (2013). doi:10.1016/j.chemgeo.2013.08.002

62. G. M. Marion, R. E. Farren, Mineral solubilities in the Na-K-Mg-Ca-Cl-SO_4-H_2O system: A re-evaluation of the sulfate chemistry in the Spencer-Moller-Weare model. *Geochim. Cosmochim. Acta* **63**, 1305–1318 (1999). doi:10.1016/S0016-7037(99)00102-7

63. A. M. Baldridge, S. J. Hook, J. K. Crowley, G. M. Marion, J. S. Kargel, J. L. Michalski, B. J. Thomson, C. R. de Souza Filho, N. T. Bridges, A. J. Brown, Contemporaneous deposition of phyllosilicates and sulfates: Using Australian acidic saline lake deposits to describe geochemical variability on Mars. *Geophys. Res. Lett.* **36**, L19201 (2009). doi:10.1029/2009GL040069

64. K. C. Benison, B. B. Bowen, Acid saline lake systems give clues about past environments and the search for life on Mars. *Icarus* **183**, 225–229 (2006). doi:10.1016/j.icarus.2006.02.018

65. J. M. McArthur, J. V. Turner, W. B. Lyons, A. O. Osborn, M. F. Thirlwall, Hydrochemistry on the Yilgarn Block, western Australia: Ferrolysis and mineralization in acidic brines. *Geochim. Cosmochim. Acta* **55**, 1273–1288 (1991). doi:10.1016/0016-7037(91)90306-P

66. K. M. Bohacs, A. R. Carroll, J. E. Neal, P. J. Mankiewicz, in *Lake Basins Through Space and Time*, E. H. Gierlowski, K. R. Kelts, Eds. (American Association of Petroleum Geologists, Tulsa, OK, 2000), vol. 46, pp. 3–34.

67. R. V. Demicco, L. A. Hardie, Eds., *Sedimentary Structures and Early Diagenetic Features of Shallow Marine Carbonate Deposits* (Society for Sedimentary Geology, Tulsa, OK, 1994), vol. 1.

68. J. Grotzinger, J. Bell, K. Herkenhoff, J. Johnson, A. Knoll, E. McCartney, S. McLennan, J. Metz, J. Moore, S. Squyres, R. Sullivan, O. Ahronson, R. Arvidson, B. Joliff, M. Golombek, K. Lewis, T. Parker, J. Soderblom, Sedimentary textures formed by aqueous processes, Erebus crater, Meridiani Planum, Mars. *Geology* **34**, 1085–1088 (2006). doi:10.1130/G22985A.1

69. B. C. Schreiber, M. El Tabakh, Deposition and early alteration of evaporites. *Sedimentology* **47**, 215–238 (2000). doi:10.1046/j.1365-3091.2000.00002.x

70. B. W. Logan, *The Macleod Evaporite Basin, Western Australia: Holocene Environments, Sediments, and Geological Evolution, Memoir No. 44* (American Association of Petroleum Geologists, Tulsa, OK, 1987).

71. J. E. Adams, M. L. Rhodes, Dolomitization by seepage refluxion. *Am. Assoc. Pet. Geol. Bull.* **44**, 1912–1920 (1960).

72. A. B. Al-Helal, F. F. Whitaker, Y. T. Xiao, Reactive transport modeling of brine reflux: Dolomitization, anhydrite precipitation, and porosity evolution. *J. Sediment. Res.* **82**, 196–215 (2012). doi:10.2110/jsr.2012.14

73. G. D. Jones, P. L. Smart, F. F. Whitaker, B. J. Rostron, H. G. Machel, Numerical modeling of reflux dolomitization in the Grosmont platform complex (Upper Devonian), Western Canada sedimentary basin. *Am. Assoc. Pet. Geol. Bull.* **87**, 1273–1298 (2003).

74. P. E. Potter, J. B. Maynard, W. A. Pryor, *Sedimentology of Shale: Study Guide and Reference Source* (Springer, 1980).

75. W. Stumm, G. F. Lee, Oxygenation of ferrous iron. *Ind. Eng. Chem.* **53**, 143–146 (1961). doi:10.1021/ie50614a030

76. R. D. Wordsworth, L. Kerber, R. T. Pierrehumbert, F. Forget, J. W. Head, Comparison of "warm and wet" and "cold and icy" scenarios for early Mars in a 3-D climate model. *J. Geophys. Res.* **120**, 1201–1219 (2015). doi:10.1002/2015JE004787

77. M. H. Carr, J. W. Head III, Geologic history of Mars. *Earth Planet. Sci. Lett.* **294**, 185–203 (2010). doi:10.1016/j.epsl.2009.06.042

78. J. Laskar, A. C. M. Correia, M. Gastineau, F. Joutel, B. Levrard, P. Robutel, Long term evolution and chaotic diffusion of the insolation quantities of Mars. *Icarus* **170**, 343–364 (2004). doi:10.1016/j.icarus.2004.04.005

79. J. P. Bibring, Y. Langevin, J. F. Mustard, F. Poulet, R. Arvidson, A. Gendrin, B. Gondet, N. Mangold, P. Pinet, F. Forget, M. Berthé, J.-P. Bibring, A. Gendrin, C. Gomez, B. Gondet, D. Jouglet, F. Poulet, A. Soufflot, M. Vincendon, M. Combes, P. Drossart, T. Encrenaz, T. Fouchet, R. Merchiorri, G. Belluci, F. Altieri, V. Formisano, F. Capaccioni, P. Cerroni, A. Coradini, S. Fonti, O. Korablev, V. Kottsov, N. Ignatiev, V. Moroz, D. Titov, L. Zasova, D. Loiseau, N. Mangold, P. Pinet, S. Douté, B. Schmitt, C. Sotin, E. Hauber, H. Hoffmann, R. Jaumann, U. Keller, R. Arvidson, J. F. Mustard, T. Duxbury, F. Forget, G. Neukum, Global mineralogical and aqueous mars history derived from OMEGA/Mars Express data. *Science* **312**, 400–404 (2006). doi:10.1126/science.1122659 Medline

80. C. Freissinet, D. P. Glavin, P. R. Mahaffy, K. E. Miller, J. L. Eigenbrode, R. E. Summons, A. E. Brunner, A. Buch, C. Szopa, P. D. Archer Jr., H. B. Franz, S. K. Atreya, W. B. Brinckerhoff, M. Cabane, P. Coll, P. G. Conrad, D. J. Des Marais, J. P. Dworkin, A. G. Fairén, P. François, J. P. Grotzinger, S. Kashyap, I. L. Ten Kate, L. A. Leshin, C. A. Malespin, M. G. Martin, F. J. Martin-Torres, A. C. McAdam, D. W. Ming, R. Navarro-González, A. A. Pavlov, B. D. Prats, S. W. Squyres, A. Steele, J. C. Stern, D. Y. Sumner, B. Sutter, M.-P. Zorzano, Organic molecules in the Sheepbed Mudstone, Gale Crater, Mars. *J. Geophys. Res. Planets* **120**, 495–514 (2015). doi:10.1002/2014JE004737 Medline

81. K. E. Miller, J. L. Eigenbrode, C. Freissinet, D. P. Glavin, B. Kotrc, P. Francois, R. E. Summons, Potential precursor compounds for chlorohydrocarbons detected in Gale Crater, Mars, by the SAM instrument suite on the Curiosity Rover. *J. Geophys. Res.* **121**, 296–308 (2016). doi:10.1002/2015JE004939

82. J. C. Stern, B. Sutter, C. Freissinet, R. Navarro-González, C. P. McKay, P. D. Archer Jr., A. Buch, A. E. Brunner, P. Coll, J. L. Eigenbrode, A. G. Fairen, H. B. Franz, D. P. Glavin, S. Kashyap, A. C. McAdam, D. W. Ming, A. Steele, C. Szopa, J. J. Wray, F. J. Martín-Torres, M.-P. Zorzano, P. G. Conrad, P. R. Mahaffy, MSL Science Team, Evidence for indigenous nitrogen in sedimentary and aeolian deposits from the Curiosity rover

investigations at Gale crater, Mars. *Proc. Natl. Acad. Sci. U.S.A.* **112**, 4245–4250 (2015). doi:10.1073/pnas.1420932112 Medline

83. R. Gellert, Mars Science Laboratory Alpha Particle X-Ray Spectrometer RDR data V1.0, MSL-M-APXS-4/5-RDR-V1.0 (NASA Planetary Data System, 2013).

84. J. L. Campbell, G. M. Perrett, R. Gellert, S. M. Andrushenko, N. I. Boyd, J. A. Maxwell, P. L. King, C. D. M. Schofield, Calibration of the Mars Science Laboratory Alpha Particle X-ray Spectrometer. *Space Sci. Rev.* **170**, 319–340 (2012). doi:10.1007/s11214-012-9873-5

85. D. Vaniman, Mars Science Laboratory Chemistry and Mineralogy RDR data V1.0, MSL-M-CHEMIN-5-RDR-V1.0 (NASA Planetary Data System, 2012).

86. D. E. Smith, M. T. Zuber, H. V. Frey, J. B. Garvin, J. W. Head, D. O. Muhleman, G. H. Pettengill, R. J. Phillips, S. C. Solomon, H. J. Zwally, W. B. Banerdt, T. C. Duxbury, M. P. Golombek, F. G. Lemoine, G. A. Neumann, D. D. Rowlands, O. Aharonson, P. G. Ford, A. B. Ivanov, C. L. Johnson, P. J. McGovern, J. B. Abshire, R. S. Afzal, X. Sun, Mars Orbiter Laser Altimeter: Experiment summary after the first year of global mapping of Mars. *J. Geophys. Res.* **106**, 23689–23722 (2001). doi:10.1029/2000JE001364

87. S. M. Chemtob, B. L. Jolliff, G. R. Rossman, J. M. Eiler, R. E. Arvidson, Silica coatings in the Ka'u Desert, Hawaii, a Mars analog terrain: A micromorphological, spectral, chemical, and isotopic study. *J. Geophys. Res.* **115**, E04001 (2010). doi:10.1029/2009JE003473

88. R. V. Morris, G. Klingelhöfer, C. Schröder, I. Fleischer, D. W. Ming, A. S. Yen, R. Gellert, R. E. Arvidson, D. S. Rodionov, L. S. Crumpler, B. C. Clark, B. A. Cohen, T. J. McCoy, D. W. Mittlefehldt, M. E. Schmidt, P. A. de Souza Jr., S. W. Squyres, Iron mineralogy and aqueous alteration from Husband Hill through Home Plate at Gusev Crater, Mars: Results from the Mossbauer instrument on the Spirit Mars Exploration Rover. *J. Geophys. Res.* **113**, E12S42 (2008). doi:10.1029/2008JE003201

89. G. Pe-Piper, A. Karim, D. J. W. Piper, Authigenesis of titania minerals and the mobility of Ti: New evidence from pro-deltaic sandstones, Cretaceous Scotian basin, Canada. *J. Sediment. Res.* **81**, 762–773 (2011). doi:10.2110/jsr.2011.63

90. S. E. Ziemniak, E. P. Opalka, Titanium(IV) oxide phase-stability in alkaline sodium-phosphate solutions at elevated temperatures. *Chem. Mater.* **5**, 690–694 (1993). doi:10.1021/cm00029a019

91. K. G. Knauss, M. J. Dibley, W. L. Bourcier, H. F. Shaw, Ti(IV) hydrolysis constants derived from rutile solubility measurements made from 100 to 300°C. *Appl. Geochem.* **16**, 1115–1128 (2001). doi:10.1016/S0883-2927(00)00081-0

92. J. F. Rapp, S. Klemme, I. B. Butler, S. L. Harley, Extremely high solubility of rutile in chloride and fluoride-bearing metamorphic fluids: An experimental investigation. *Geology* **38**, 323–326 (2010). doi:10.1130/G30753.1

93. O. Forni, M. Gaft, M. J. Toplis, S. M. Clegg, S. Maurice, R. C. Wiens, N. Mangold, O. Gasnault, V. Sautter, S. Le Mouélic, P.-Y. Meslin, M. Nachon, R. E. McInroy, A. M. Ollila, A. Cousin, J. C. Bridges, N. L. Lanza, M. D. Dyar, First detection of fluorine on

Mars: Implications for Gale Crater's geochemistry. *Geophys. Res. Lett.* **42**, 1020–1028 (2015). doi:10.1002/2014GL062742

94. R. W. Ricker, F. A. Hummel, Reactions in the system TiO_2-SiO_2; Revision of the phase diagram. *J. Am. Ceram. Soc.* **34**, 271–279 (1951). doi:10.1111/j.1151-2916.1951.tb09129.x

95. H. Schneider, A. Majdic, Titanium incorporation in tridymite. *Neues Jahrb. Mineral.* 418–426 (1985).

96. H. Schneider, Chemical-composition of tridymite and cristobalite from volcanic and meteoritic rocks. *Neues Jahrb. Mineral.* 433–444 (1986).

97. B. Mason, Lunar tridymite and cristobalite. *Am. Mineral.* **57**, 1530–1535 (1972).

98. M. Sato, Tridymite crystals in opaline silica from Kusatsu, Gumma Prefecture. *Mineral. J.* **3**, 296–305 (1962). doi:10.2465/minerj1953.3.296

99. K. S. Edgett, R. A. Yingst, M. A. Ravine, M. A. Caplinger, J. N. Maki, F. T. Ghaemi, J. A. Schaffner, J. F. Bell, L. J. Edwards, K. E. Herkenhoff, E. Heydari, L. C. Kah, M. T. Lemmon, M. E. Minitti, T. S. Olson, T. J. Parker, S. K. Rowland, J. Schieber, R. J. Sullivan, D. Y. Sumner, P. C. Thomas, E. H. Jensen, J. J. Simmonds, A. J. Sengstacken, R. G. Willson, W. Goetz, Curiosity's Mars Hand Lens Imager (MAHLI) Investigation. *Space Sci. Rev.* **170**, 259–317 (2012). doi:10.1007/s11214-012-9910-4